



ORIGINAL ARTICLE

CuMn₂O₄/chitosan micro/nanocomposite: Green synthesis, methylene blue removal, and study of kinetic adsorption, adsorption isotherm experiments, mechanism and adsorbent capacity



Malihe Samadi Kazemi^a, Azam Sobhani^{b,*}

^a Department of Chemistry, Faculty of Sciences, Bojnourd Branch, Islamic Azad University, Bojnourd 9417697796, Iran

^b Department of Chemistry, Kosar University of Bojnord, Bojnord P. O. Box. 94104455, Republic of Iran

Received 18 October 2022; accepted 25 February 2023

Available online 2 March 2023

KEYWORDS

CuMn₂O₄;
Chitosan;
Composite;
Adsorbent;
Hydrothermal;
Methylene blue removal

Abstract In this work, we choose a simple, green hydrothermal method for the fabrication of a pure phase of CuMn₂O₄ nanostructures in the presence of onion as a capping agent, for the first time. In the next step, we synthesized CuMn₂O₄/chitosan micro/nanocomposite. The structural analysis of nanostructures and composites showed their purity. The results showed that the prepared micro/nanocomposites have very efficient adsorption for removing methylene blue. In order to design and analyze the experiments were used response surface methodology (RSM). In the optimal conditions, the pH value, adsorbent dose, initial concentration, contact time and stirring speed obtained 6.5, 1.25 g/L, 1 mg/L, 5 min and 500 rpm respectively. Kinetic adsorption and adsorption isotherm experiments were used to investigate the process mechanism and adsorption capacity of CuMn₂O₄/chitosan composites for methylene blue, for the first time. The value of R² (0.997) and the q_{e cal} which was close to the q_{e exp}, confirmed the pseudo-first-order kinetic model. Langmuir isotherm model with a q_{max} of 54.05 mg/g described the experimental data well. K_L in this model obtained 0.06, which was in the range of 0–1, which means the adsorption process CuMn₂O₄/chitosan composite for methylene blue was favorable. Moreover, the present adsorbent can be effectively used up to five adsorption/desorption cycles.

© 2023 The Authors. Published by Elsevier B.V. on behalf of King Saud University. This is an open access article under the CC BY-NC-ND license (<http://creativecommons.org/licenses/by-nc-nd/4.0/>).

* Corresponding author.

E-mail address: sobhani@kub.ac.ir (A. Sobhani).

Peer review under responsibility of King Saud University.



1. Introduction

Copper manganite (CuMn_2O_4) is a mixed metal oxide and can incorporate into the spinel structure. The XRD and neutron diffractions show that the CuMn_2O_4 has a structure of the cubic spinel and is analogous to CuFe_2O_4 (Sinha et al., 1958; Radhakrishnan and Biswas, 1974; Verwey and Heilmann, 1947; Enhessari et al., 2016; Popescu et al., 2015; Shoemaker et al., 2009). The mixed copper manganese oxides are of considerable industrial interest due to their potential application (Wollner et al., 1993; Hutchings et al., 1996). The synthesis of the pure CuMn_2O_4 is challenging. This challenge is due to the formation probability of the secondary phases of Mn. Also, the Cu^{2+} reduction can prepare Cu in the solution as an impurity. Thus choosing a suitable synthesis technique to prepare pure CuMn_2O_4 is very important. In this research, we have adopted a simple hydrothermal route to prepare the pure CuMn_2O_4 utilizing onion as a green capping agent for the first time. *Allium cepa*, commonly known as onion, is a source of various biologically active compounds and has pharmacological activity. It is a rich source of flavonoids, making it an anti-oxidant and anti-inflammatory agent. The *Allium cepa* is used as a capping agent in this work to prevent the formation of the aggregated structures.

After the synthesis of CuMn_2O_4 , we synthesized nanocomposites with chitosan. For this purpose, chitosan was added to the CuMn_2O_4 nanostructures dispersed in water to functionalize, modify and improve surface properties. Chitosan is a natural biopolymer composed of randomly distributed b-(1-4)-linked D-glucosamine (deacetylated unit) and N-acetyl-D-glucosamine (acetylated unit). There are many reports regarding the use of chitosan in food industry as additives, in indigestion tablets, in preparation of dental impressions and tissue engineering because of its positive feature with respect to non-toxicity, biocompatibility and bioavailability. Furthermore, chitosan is of pharmaceutical interest, being already used in wound healing, dermatology, anti-itching, drug delivery and tissue engineering (Yao et al., 2010; Kumar, 2000). Also, chitosan can be used as an adsorbent for dye removal from aqueous solutions due to the presence of amino and hydroxyl groups as active adsorption sites. The use of adsorbents composed of natural polymers has attracted significant interest, and polysaccharides such as chitosan and its derivatives have received particular attention (Reddy and Lee, 2013). This is due to the fact that chitosan is a low-cost and effective adsorbent compared with activated carbons and other adsorbents used in treatment organic or inorganic contaminated water (Bhatnagar and Sillanpää, 2009). There is an abundance of citations in the literature describing the performance of chitosan as an adsorbent for pollutants from water and wastewater including metals, dyes, phenols, fluoride, and phthalates (Julinová and Slavík, 2012).

This paper presents the synthesis of CuMn_2O_4 /chitosan micro/nanocomposites (CMO/C NCs). It reports detailed information on the methylene blue (MB) adsorption as dye pollution in water by these composites. There are some researchers have made to synthesize composites of CuMn_2O_4 . In 2019 Chani et al. synthesized CuMn_2O_4 -chitosan nanocomposite and showed that the as-prepared nanocomposite-based sensors can be used as sensing elements in the meters used for environmental monitoring (Chani et al., 2019). In 2021 Sheikhzadeh and Sanjabi synthesized the different compositions of copper manganese oxide films using the electrochemical deposition technique (Sheikhzadeh and Sanjabi, 2021). Sodium citrate was used as a complex agent in this synthesis. Zhang et al. synthesized CuMn_2O_4 -graphene composites as complex agents. They used two methods, including sol-gel and physical grinding, in 2021 (Zhang et al., 2021). The CuMn_2O_4 -graphene composites exhibited better cyclic stability than pure graphene and CuMn_2O_4 . CMO/C NCs prepared in this work help to remove the MB from the aqueous solution. This research is the first report of the MB removal from the aqueous solution by CMO/C NCs as an adsorbent.

The problem of water pollution is a great concern. Dye is one of the polluters of the environment due to its high use in industries such as

textile, food, cosmetic and etc. Acidic and cationic dyes are widely used in industries. MB is a cationic dye. Increased heart rate, quadriplegia, cyanosis, jaundice, shock, Heinz body formation, vomiting, and tissue necrosis are unfavorable effects on human health caused by MB (Ahmad and Kumar, 2010). Thus control of the MB contents is necessary because it is biologically dangerous. Several physicochemical technologies, including coagulation-flocculation, membrane separation, ion exchange, chemical oxidation, electrochemical techniques, adsorption and photocatalysis, have been studied for the purpose of removing MB (Allègre et al., 2006; Marrot and Roche, 2002; Holkar et al., 2016). The dye pollution elimination from the solvent phase by adsorption is a necessary research aspect (Khatooni et al., 2023; Rowshanzamir et al., 2015; Safarzadeh et al., 2022; Tehrani-Bagha et al., 2011).

This work reports the effects of contact time, and the initial concentration of MB on the removal efficiency by the adsorbent and investigates the mechanism of process and capacity of theoretical adsorbent by kinetic adsorption and adsorption isotherm experiments. To obtain the optimal conditions of the surface adsorption process, was used the response surface methodology (RSM). The effects of pH, adsorbent dosage, initial concentration of MB, contact time and agitation speed were investigated. In addition, Langmuir, Freundlich, Temkin, Dubinin-Radushkevich isotherm models were used for estimation of the adsorption capacity of CMO/C NCs. Furthermore, the kinetic studies using the pseudo-first-order, pseudo-second-order, Elovich and intraparticle diffusion kinetic models were accomplished to explain the adsorption process and to determine kinetic coefficients.

The development of a simple and economical route for obtaining nanostructures coated with biopolymers is an important topic and represents the purpose of this study. We used chitosan due to its favorable adsorption properties and large surface area to develop an adsorbent. We found it to be very effective. In this work, taking advantage of the various features of chitosan, our purpose was the preparation of an organic-inorganic composite as a novel adsorbent for MB removal. Despite having less stability as compared to inorganic materials the organic materials are very attractive because of their low density, high flexibility, large surface area and simple fabrication. So, the use of organic-inorganic composite for dye pollution removal is very fascinating.

2. Experimental

2.1. Materials and methods

$\text{Cu}(\text{NO}_3)_2 \cdot 3\text{H}_2\text{O}$, $\text{Mn}(\text{NO}_3)_2 \cdot 4\text{H}_2\text{O}$, and NH_3 (25%) from Merck company were purchased. An X-ray diffractometer, Philips X'pertPro with Ni-filtered $\text{Cu K}\alpha$ radiation and $\lambda = 1.54 \text{ \AA}$, was used to study XRD patterns. The morphologies of the products by field emission scanning (SEM) and transmission (TEM) electron microscopes studied, TESCAN Mira3 FE-SEM and Philips EM208 with 200 kV voltage. Nicolet IS 10 and Evolution 300 spectrophotometers made by the American Thermo scientific company were used to investigate FT-IR and UV-Vis spectra. A VSM (vibrating sample magnetometer) Meghnatis Kavir Kashan Co. made in Kashan (Iran) was used to study the magnetic property of the products.

2.2. Synthesis of CuMn_2O_4 nanostructures

Hydrothermal is a simple, low-cost, and environmentally friendly process (Emadi et al., 2017; Sobhani and Salavati-Niasari, 2021; Salavati-Niasari and Sobhani, 2013; Sobhani et al., 2012; Sobhani and Salavati-Niasari, 2015; Sobhani and Salavati-Niasari, 2014). This route is applied to synthesize the CuMn_2O_4 nanostructures in this research. First, Cu

(NO₃)₂·3H₂O and Mn(NO₃)₂·4H₂O were dissolved in water, with a stoichiometric ratio of 1:2. Then, onion and NH₃ were added drop-wise to the above precursor solution under magnetic stirring. After 25 min stirring, the pH was adjusted to 9 by ammonia. Afterward, the obtained solution was transferred into an autoclave and maintained at 180 °C for 12 h. Then autoclave cooled at the rate of 1 °C/min, and the product was washed with ethanol and distilled water and dried at 60 °C.

2.3. Synthesis of CuMn₂O₄/chitosan micro/nanocomposites

To prepare CMO/C NCs, first, chitosan was dissolved in acetic acid and distilled water. Then CuMn₂O₄ was dispersed in distilled water and added to the chitosan solution. The weight ratio of Cu: chitosan was selected 1:1. After 24 h stirring and vaporization of the water of the reaction mixture, the product was washed with distilled water and then ethanol. The obtained composites dried at 60 °C temperature (under vacuum).

2.4. Adsorption experiments using CCD model

In this study, the optimization of the MB adsorption onto the prepared adsorbent was accomplished by the response surface methodology of central composite design (RSM – CCD). Hence, pH, adsorbent dosage, MB concentration, contact time and agitation speed were investigated as the independent variables at three levels (–1, 0, + 1), and the removal efficiency of MB was considered as the response factor. Table 1 represents the levels of the three independent variables. Data was analyzed using Design-Expert software version 13 (Stat-ease, Inc., Minneapolis, MN, USA).

2.5. Kinetic adsorption experiments

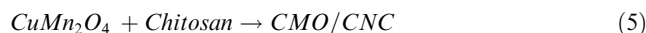
Adsorption kinetic models, in addition to determining the adsorption rate, have the ability to predict the adsorption process with time. In order to investigate the effect of contact time on the MB removal from aqueous mediums, the experiments done in 8 beakers. 0.05 g of CMO/C Nc, as adsorbent, and 40 mL of the MB solution with a concentration of 1 mg/L were added to each of the beakers. Then pH was adjusted to 6.5. The solutions were placed on a shaker for 5, 10, 30, 60, 90, 120, and 180 min. After the mentioned times, the adsorbent was separated from the solution using filter paper. Then the residual concentration of MB in the solution was measured using a UV–Vis spectroscopy at λ_{max} = 668 nm. In order to study the effect of the initial concentration of MB on the equilibrium time, the above steps were performed on concentrations of 2, 5, 10, 25, 50, and 80 mg/L.

Table 1 The levels of factors in the RSM-CCD model.

Variable	Symbol	Low	High	Levels
pH	A	1	12	1,6,5,12
Adsorbent dosage (g/L)	B	1.25	3	1.25,2,15,3
Contact time (min)	C	5	120	5,62,120
Agitation speed (rpm)	D	100	500	100,300,500
MB concentration (mg/L)	E	1	80	1,40,80

3. Results and discussion

The main reactions relate to the formation of CuMn₂O₄ and CMO/C NC can be summarized as follows:



It was found from XRD data that the product formed from Cu(NO₃)₂·3H₂O and Mn(NO₃)₂·4H₂O in the presence of onion and NH₃, after 12 h hydrothermal reaction at 180 °C, is the pure CuMn₂O₄. Fig. 1a shows the XRD pattern of CuMn₂O₄ and confirms the formation of the monoclinic phase of CuMn₂O₄ (JCPDS card No. 00–010 – 0365) and correspond to diffractions from the (002), (–201), (–110), (–111), (201), (202), (–113), (–311) and (113) planes at angles 2theta of 31.362, 33.027, 35.308, 36.96, 40.227, 51.784, 57.052, 59.179 and 64.378, respectively. Fig. 1b shows the XRD pattern of CMO/C NC. The diffraction peaks of CuMn₂O₄ in this figure observe at lower thetas after the coating with chitosan and the formation of the composites. XRD studies have shown that raw chitosan itself is amorphous (Zhu et al., 2010). Fig. 1b shows broader peaks and lower intensities than those in Fig. 1a, which are the signs of lower crystallinity of the composites than the nanostructures. The CuMn₂O₄ is bonded to the chitosan matrix via hydroxyl and amine groups of the chitosan. It causes the three-dimension structure of the composites to be more disordered. Thus the XRD peaks of CuMn₂O₄, in Fig. 1b, are not identified clearly. Fig. 1c shows the EDS spectrum of sample 6. The peaks of Cu, Mn, and O with atomic percents 12.74, 23.05, and 64.22 % are observed in this figure, and confirms the formation of CuMn₂O₄.

The size and morphology of CuMn₂O₄ and CMO/C NCs examined by SEM microscope. Fig. 2a-c shows SEM images of CuMn₂O₄ prepared in this work in the different magnifications. The figures illustrate the formation of the microspheres and spherical nanoparticles with diameters of 1–5 μm and 100–300 nm, respectively. SEM image with high magnification in Fig. 2c shows the formation of the agglomerated nanoparticles and microspheres coated by nanoparticles with diameters lower than 10 nm. SEM images of CMO/C NCs in Fig. 2d-f reveal that the chitosan coating does not result in the morphology change. These images show the formation of the microspheres with diameters of 1.5–6 μm and agglomerated nanoparticles with the irregular distribution. Careful observation of the magnified SEM image in Fig. 2f shows that the surfaces of the spheres are not smooth. TEM image was also taken to characterize the morphology of the nanocomposites. This image in Fig. 2g shows the formation of the spheres with diameters ~ 800 nm.

Fig. 3a shows the hysteresis curve of CMO/C NCs prepared in the present work at room temperature. Superexchange interactions between Mn³⁺–O^{2–}–Mn⁴⁺ (B–B interaction) and Mn³⁺–O^{2–}–Cu²⁺ (A–B interaction), and also the orientation of the site of Mn and Cu in copper manganite spinel is the

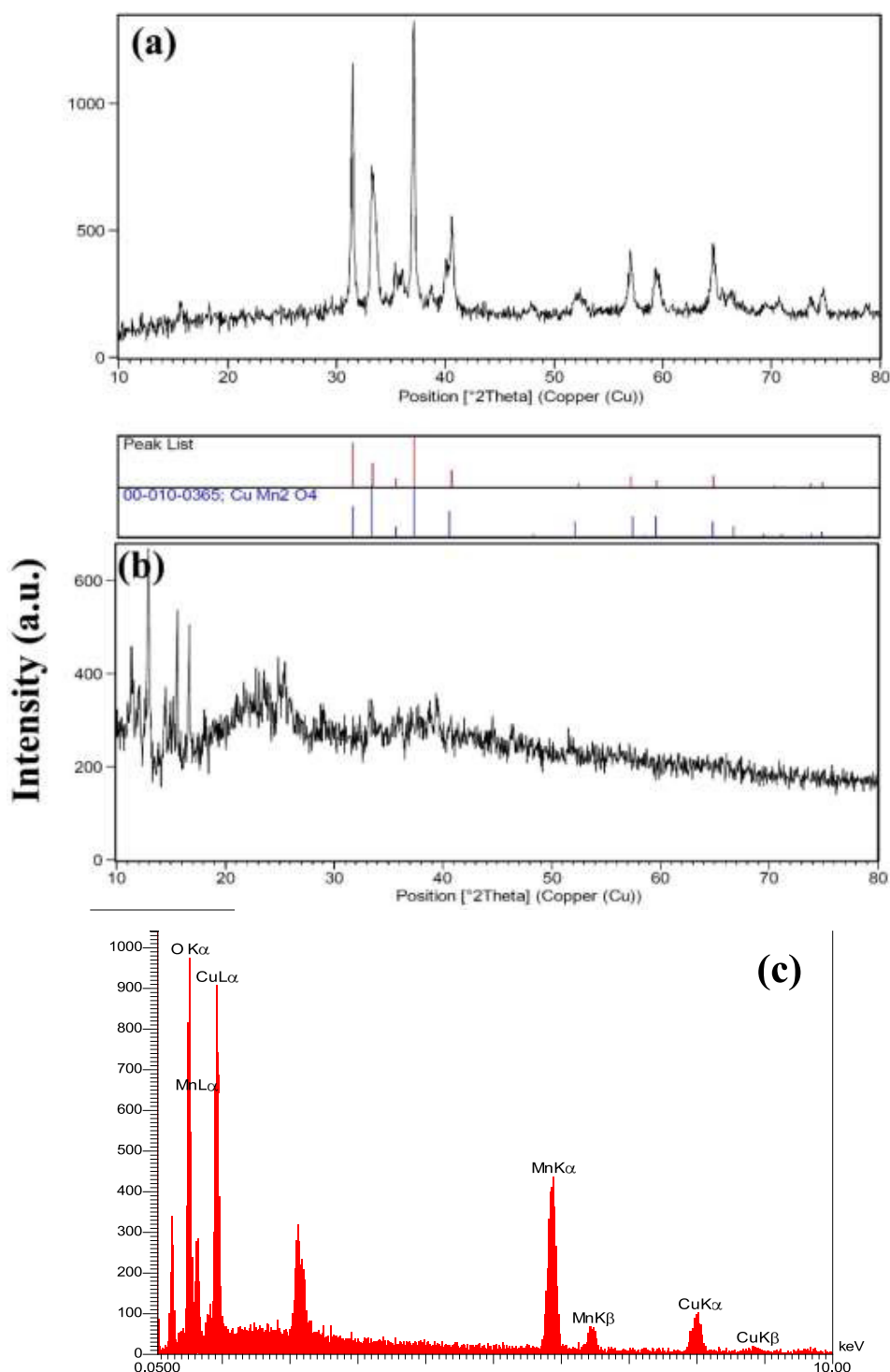


Fig. 1 XRD patterns from: (a) the product prepared from $\text{Cu}(\text{NO}_3)_2 \cdot 3\text{H}_2\text{O}$ and $\text{Mn}(\text{NO}_3)_2 \cdot 4\text{H}_2\text{O}$ in the presence of onion and NH_3 , after 12 h hydrothermal reaction at 180°C (sample 6) and (b) the composite prepared from CuMn_2O_4 and chitosan, (c) EDS spectrum of sample 6.

cause of magnetic properties of them (Waskowska et al., 2001; Shoemaker et al., 2009; Buhl, 1969; Vandenberghe et al., 1976). The magnetic measurements carried out by the VSM magnetometer show a pretty weak ferromagnetic behavior in low fields in Fig. 3a. This behavior is because grains in composites may pose uncompensated moments. According to the M–H plot, the coercivity is approximately 179 Oe. In contrast,

an antiferromagnetic behavior shows for the composites in high fields. The antiferromagnetic behavior of CMO/C NC can be due to the $\text{Mn}^{n+1}/\text{Mn}^{n+}$ redox couple located in the B-sites of the spinels. (Verwey, 1951).

This work investigates the effect of the capping agent. Details of the capping agent study have been described in the author's published article (Sobhani, 2022). In the absence

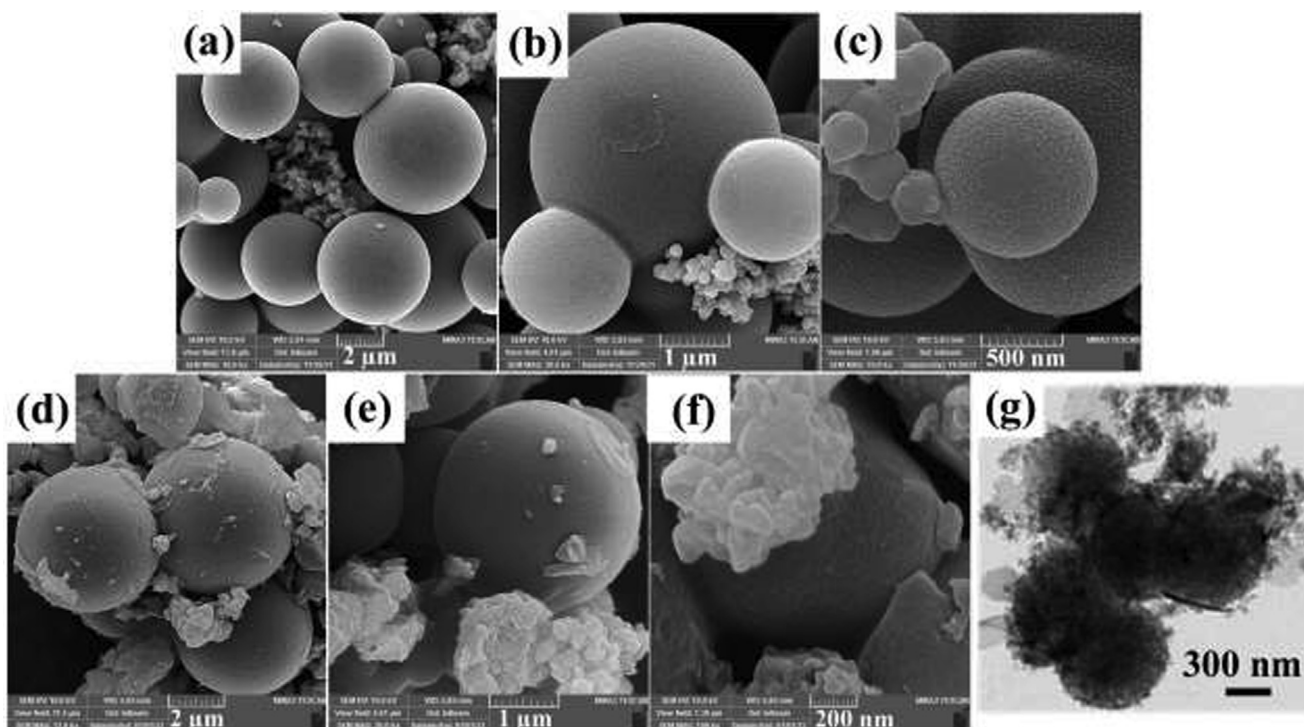


Fig. 2 SEM images in the different magnifications of: (a-c) CuMn₂O₄ nanostructures and (d-f) CMO/C NCs, (g) TEM image of CMO/C NCs.

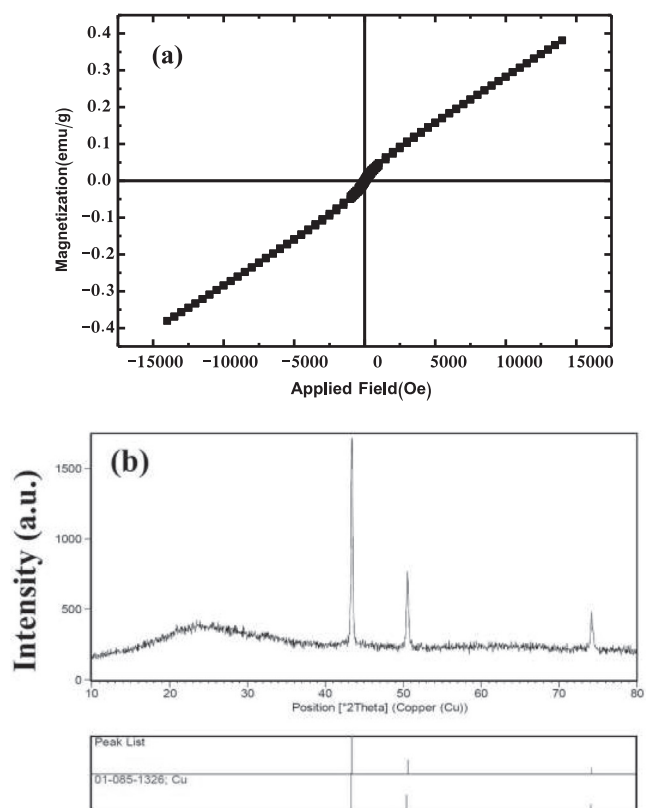


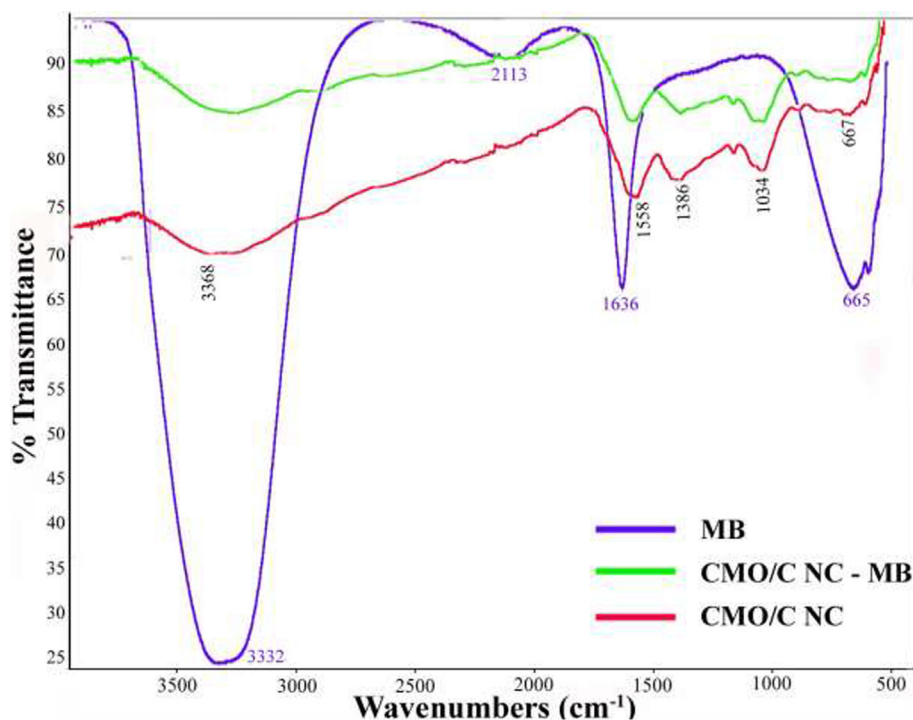
Fig. 3 (a) Hysteresis curve of CMO/C NC, (b) XRD pattern from the product prepared from Cu(NO₃)₂·3H₂O and Mn(NO₃)₂·4H₂O after 12 h hydrothermal reaction at 180 °C, in the presence of onion and in the absence of NH₃.

of the capping agent, CuMn₂O₄ and a small amount of CuO impurity are products. Maleic acid, glucose, maltose, and phenylalanine were also used as capping agents. The products prepared with maleic acid were both Cu and MnCO₃. The Cu₂O, Mn₃O₄, and Cu were the products formed in the presence of glucose and maltose, respectively. With phenylalanine, the formation of a small percentage of CuMn₂O₄ and Mn₃O₄ was observed. Thus maleic acid, glucose, maltose, and phenylalanine were not suitable capping agents to synthesize the copper manganite spinels. Also, the copper manganite formed in the absence of the capping agent was impure. But in this work, we prepared pure CuMn₂O₄, in the presence of onion as a green capping agent. Thus onion was known as the optimized capping agent in this work. The reaction conditions to synthesize the copper manganites have been listed in Table 2. To prepare CMO/C NCs, the CuMn₂O₄ prepared in the presence of onion was dispersed in distilled water and added to the chitosan solution. Also, in this study effect of pH on the product type was investigated. The XRD pattern in Fig. 3b shows the formation of the pure Cu with cubic crystal structure and JCPDS card No. 01-085-1326 in the absence of NH₃. Thus pH and capping agents are effective agents to synthesize pure copper manganites.

The FT-IR spectrum identified functional groups in the composites and proved MB adsorption on the surface of CMO/C NC. The FT-IR spectra were recorded in the wavelength range 500–4000 cm⁻¹, as shown in Fig. 4. The red curve in Fig. 4 shows the FT-IR spectrum of CMO/C NC. In this curve, the frequencies below 1000 cm⁻¹ belong to the M–O stretching vibrations (Wang et al., 2013). The vibrational bands at about 600–800 cm⁻¹ confirm the formation of Mn–O and Cu–O bands in the as-prepared composite (Abel

Table 2 The reaction conditions of copper manganites synthesized in this work.

Sample	Cu source	Mn source	NH ₃	Capping agent	Temperature (C)	Time	Product
1	Cu(NO ₃) ₂ ·3H ₂ O	Mn(NO ₃) ₂ ·4H ₂ O	✓	–	180	12	CuMn ₂ O ₄ / CuO
2	Cu(NO ₃) ₂ ·3H ₂ O	Mn(NO ₃) ₂ ·4H ₂ O	✓	Maleic acid	180	12	Cu + MnCO ₃
3	Cu(NO ₃) ₂ ·3H ₂ O	Mn(NO ₃) ₂ ·4H ₂ O	✓	Glucose	180	12	Cu ₂ O + Mn ₃ O ₄
4	Cu(NO ₃) ₂ ·3H ₂ O	Mn(NO ₃) ₂ ·4H ₂ O	✓	Maltose	180	12	Cu
5	Cu(NO ₃) ₂ ·3H ₂ O	Mn(NO ₃) ₂ ·4H ₂ O	✓	Phenylalanine	120	12	CuMn ₂ O ₄ + Mn ₃ O ₄ + Impurity
6	Cu(NO ₃) ₂ ·3H ₂ O	Mn(NO ₃) ₂ ·4H ₂ O	✓	Onion	180	12	pure CuMn ₂ O ₄
7	Cu(NO ₃) ₂ ·3H ₂ O	Mn(NO ₃) ₂ ·4H ₂ O	–	Onion	180	12	Cu

**Fig. 4** FT-IR spectra of the MB, CMO/C NC, and MB adsorbed on the surface of CMO/C NC.

et al., 2019). The bands centered at 1386 and 1034 cm^{-1} show the existence of some organic residues in the composites (C-OH groups) (Ma et al., 2016). Also, the two peaks at 1601 and 1558 cm^{-1} in the red curve correspond to C=O and C-O vibrational modes. The broad peak in the range 2800–3600 cm^{-1} (including 3368 cm^{-1}) in this curve is related to the stretching vibrations of absorption water on the surface of the composites. The blue and green curves in Fig. 4 are FT-IR spectra of MB and adsorbed MB on the CMO/C NC surface, respectively. The blue curve shows high-intensity peaks of MB. These peaks disappear after the MB adsorption on the CMO/C NC surface. Before and after the adsorption of MB on the surface of the composite, FT-IR spectra of the composite are similar, and only peaks are blue-shifted in the spectrum of the composite after MB absorption. The FT-IR results in Fig. 4 confirm the application of as-prepared CMO/C NC as an effective adsorbent for MB removal from an aqueous solution.

Fig. 5 shows the UV-Vis absorbance spectra of pure MB solution and MB solution in the presence of CMO/C NC. The spectra are in the 200–800 nm range. The red curve in

Fig. 5 is the UV-Vis spectrum of pure MB solution. It is characterized by three bands, one in the visible region ($\lambda_{\text{max}} \sim 670 \text{ nm}$) and two in the UV region ($\lambda_{\text{max}} \sim 290 \text{ nm}$ and $\lambda_{\text{max}} \sim 250 \text{ nm}$). The absorbance spectrum of the MB solution displays maximum absorption at about 670 nm. The blue curve in Fig. 5 is related to the absorbance spectrum of MB solution in the presence of CMO/C NC. As seen in this figure, three UV-Vis bands of MB disappear with CMO/C NCs, because of MB adsorption on the surface of the micro/nanocomposites. In other words, after adding CMO/C NC into the MB solution, all dye is adsorbed by CMO/C photocatalyst. The amino and hydroxyl groups in chitosan help MB adsorption and degradation. Therefore, UV-Vis results in Fig. 5 confirm the application of as-prepared CMO/C NC as a very effective adsorbent for MB removal from wastewater. Also, the photo taken from the MB solution before and after adding CMO/C NC as an adsorbent (inserted in Fig. 5) shows that the blue color of MB completely disappeared after adding CMO/C NC. Scheme 1 shows schematic synthesis, characterization, and application of as-prepared CMO/C NCs in MB removal from aqueous solution. The dyes removal from aque-

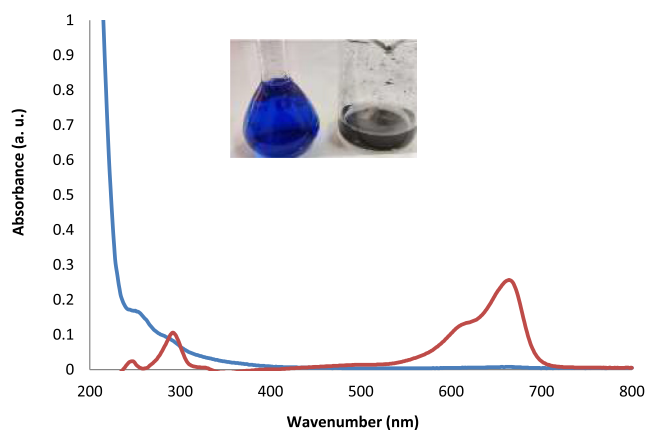


Fig. 5 The absorbance spectra of MB (red curve) and MB adsorbed on the surface of CMO/C NC (blue curve).

ous environments using metal oxide spinels has been investigated by many researchers (Ahmadi et al., 2022). The spinels of metal oxides with the general composition AB₂O₄, in which A may be magnesium, iron, zinc, manganese, nickel, and so on; B may be aluminum, chromium, manganese, iron, and so on; and O is oxygen have been used to remove dyes (Foroutan et al., 2021).

Variance analysis for MB removal percent is provided based on pH, adsorbent dosage, MB concentration, contact time, and agitation speed in Table 3. P-values more than 0.1 indicate that variables do not affect the process, while P-values lower than 0.05 prove that the parameters are essential. According to Table 3, A, B, E, AE, BC, BE, CE, DE, A² are significant model terms.

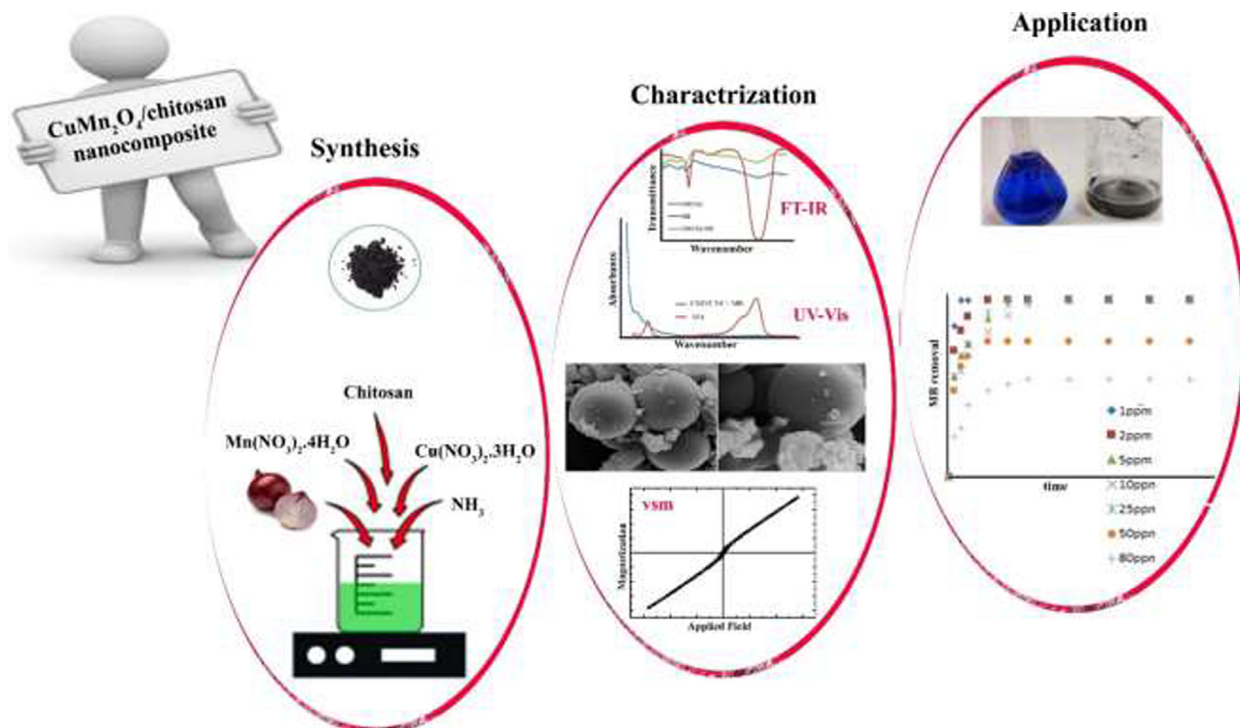
The R² amount of more than 0.8, refers that the empirical data's desired agreement with the obtained one by the relevant equations (Fereidonian Dashti et al., 2018). The result show (Table 3), the predicted R² (0.9729) is close to the adjusted R² (0.9983). Based on this Table Lack of fit is not significant with the Lack of Fit F-value of 2.30.

The equation for predicting the optimum point was obtained according to the central composite design and input variables, and then the empirical relationship between the response and the independent variables in the coded units was presented on the basis of the experimental results as follows:

$$\text{MB removal (\%)} = 98.32 - 4.04A - 0.8885B + 0.8072C - 0.1197D - 1.63E + 0.4134AB - 0.0501AC - 0.4543AD - 1.84AE + 1.09BC + 0.6491BD - 1.71BE - 0.4879CD + 2.40CE + 1.58DE - 68.65A^2 + 0.6530B^2 - 0.0037C^2 - 0.5970D^2 - 1.03E^2.$$

In the optimal conditions for the surface absorption process of MB, the pH value, adsorbent dose, initial concentration, contact time and stirring speed obtained 6.5, 1.25 g/L, 1 mg/L, 5 min and 500 rpm respectively. In these conditions, the removal percentage value of 98.98% was obtained with a desirability equal to 1, which indicates the approval of the model for the removal of MB with CMO/C NCs adsorbent.

Three-dimensional response surfaces of MB removal percent versus significant variables are presented in Fig. 6 a-c. As can be seen from Fig. 6a, c, the effect of pH is on the removal percentage more than the adsorbent dose and the initial concentration of MB. In Fig. 6a, the amount of response is plotted versus pH and adsorbent dosage. In acidic mediums, the removal of MB decreases, this decrease may be due to the presence of an additional amount of H⁺ compared to MB dye (as a cationic dye) for adsorption on the adsorbent



Scheme 1 Diagram illustrating the synthesis, characterization, and application of CMO/C NCs for MB removal from aqueous solution.

Table 3 ANOVA values in the RSM-CCD model for MB removal percent.

Source	Sum of Squares	df	Mean Square	F-value	p-value	
Model	38648.25	20	1932.41	895.66	< 0.0001	significant
A	279.78	1	279.78	129.68	< 0.0001	
B	10.80	1	10.80	5.01	0.0469	
C	8.92	1	8.92	4.13	0.0669	
D	0.2454	1	0.2454	0.1137	0.7423	
E	29.50	1	29.50	13.67	0.0035	
AB	2.59	1	2.59	1.20	0.2969	
AC	0.0379	1	0.0379	0.0176	0.8969	
AD	2.44	1	2.44	1.13	0.3103	
AE	39.00	1	39.00	18.08	0.0014	
BC	14.14	1	14.14	6.55	0.0265	
BD	6.38	1	6.38	2.96	0.1135	
BE	27.47	1	27.47	12.73	0.0044	
CD	3.60	1	3.60	1.67	0.2227	
CE	53.83	1	53.83	24.95	0.0004	
DE	28.64	1	28.64	13.27	0.0039	
A ²	11836.30	1	11836.30	5486.03	< 0.0001	
B ²	1.07	1	1.07	0.4964	0.4957	
C ²	0.0000	1	0.0000	0.0000	0.9969	
D ²	0.8951	1	0.8951	0.4149	0.5327	
E ²	2.59	1	2.59	1.20	0.2963	
Residual	23.73	11	2.16			
Lack of Fit	17.42	6	2.90	2.30	0.1895	not significant
Pure Error	6.31	5	1.26			
Cor Total	38671.98	31				
R ² : 0.9994						
Adjusted R ² : 0.9983						
Predicted R ² : 0.9729						

sites. In high pH the removal percent due to the change in the structure of the adsorbent or MB reduced. Travlou et al. (Travlou et al., 2013) studied the effect of pH on adsorption-desorption of reactive dye by GO-Chm. They reported that reactive dye adsorption decreased from 81% to 35% with the increase of pH from 3 to 12 and desorption occurred under alkaline conditions (pH 12).

The adsorption capacity of MB at the time, t (q_t (mg/g)) and equilibrium (q_e (mg/g)) was calculated by the following Eqs. (6) and (7) (Far et al., 2020; Gollakota et al., 2021; Khan et al., 2021):

$$q_t = \frac{(C_0 - C_t)V}{m} \quad (6)$$

$$q_e = \frac{(C_0 - C_e)V}{m} \quad (7)$$

C_0 , C_e , and C_t (mg/L) are concentrations at the initial, equilibrium, and time t , respectively. m (g) is the adsorbent mass, and V (L) represents the solution volume. The dye removal efficiency as follows is calculated (Guimaraes et al., 2020; Wang et al., 2020):

$$\text{Removal}\% = \frac{(C_0 - C_e)}{C_0} \times 100 \quad (8)$$

The kinetic behavior studies of the adsorption process can provide valuable information about the equilibrium state of the operation (Alizadeh et al., 2022; Foroutan et al., 2022). Different models such as pseudo-first-order, pseudo-second-order, and Elovich model can be used to survey the kinetic behavior. Among these models, the pseudo-first-order and

pseudo-second-order are extensively used to determine the physical or chemical interactions between the contaminant ions and the adsorbent surface (Foroutan et al., 2022). In this study, the kinetic models of pseudo-second-order, pseudo-second-order, intra-particle diffusion, and Elovich have been used. Their linear formulas are given in equations (9)–(12), respectively (Ahmadijokani et al., 2020; Yin et al., 2020).

$$\ln(q_e - q_t) = \ln(q_e) - K_1 t \quad (9)$$

$$\frac{t}{q_t} = \frac{1}{K_2 q_e^2} + \frac{t}{q_e} \quad (10)$$

$$q_t = K_{id} t^{1/2} + C \quad (11)$$

$$q_t = A + B \ln t \quad (12)$$

q_t and q_e (mg/g) are the mass of adsorbent at t and the equilibrium times, respectively. The k_1 (min^{-1}), k_2 ($\text{g mg}^{-1} \text{min}^{-1}$), k_{id} ($\text{mg/g min}^{1/2}$), and A (mg/g , min) and B (g/mg) are the rate coefficient of pseudo-first-order, pseudo-second-order, intra-particle diffusion, and Elovich models, respectively. The C is the dimensionless constant related to the thickness of the boundary layer.

Isotherms of Langmuir, Freundlich, Temkin, and Dubinin-Radushkevich were applied to investigate the process mechanism of the theoretical adsorbent capacity (Pamukoglu and Kargi, 2006; Pamukoglu and Kargi, 2007). Based on the Langmuir model, the adsorbate species homogeneously cover the surface to form a regular monolayer. Freundlich model assumes the multilayer coverage of adsorbate onto the heterogeneous adsorbent surface. The linear forms of the Langmuir,

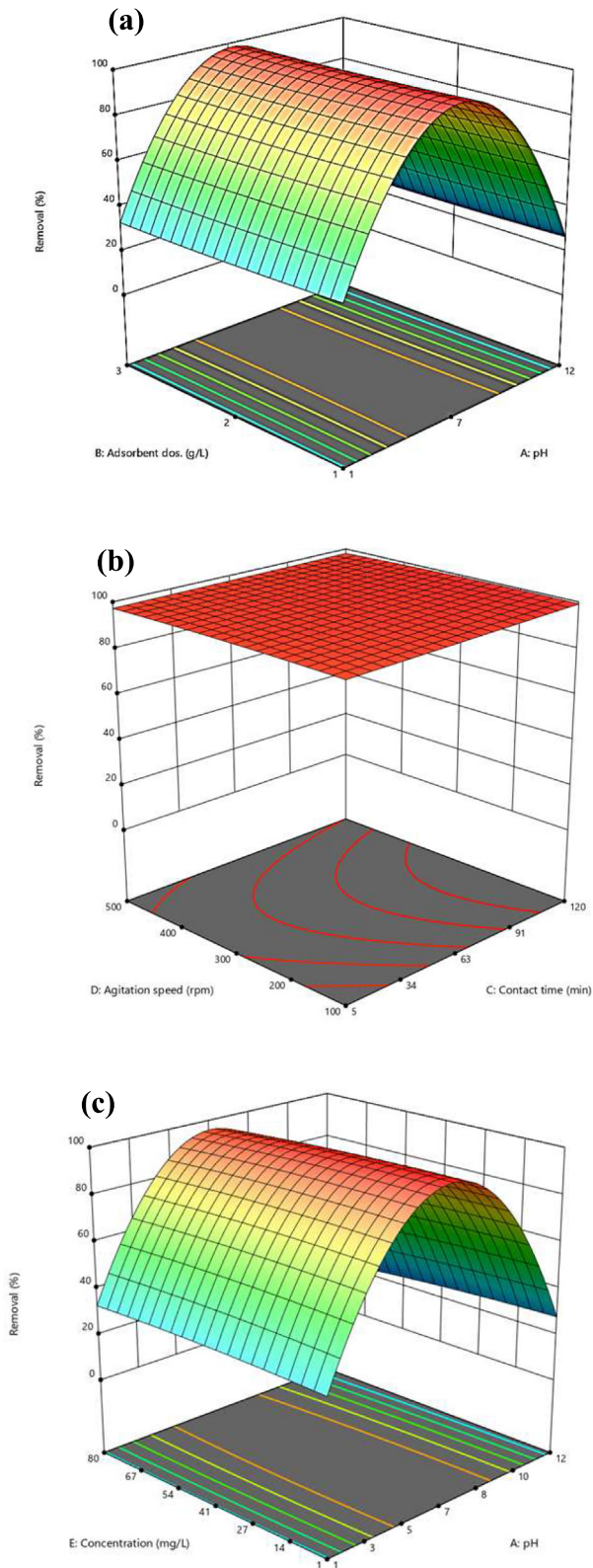


Fig. 6 The 3D graph for (a) influence of pH and adsorbent dosage (b) influence of contact time and agitation speed (c) influence of concentration and pH on phenol removal percent.

Freundlich, Temkin, and Dubinin-Radushkevich models have shown below, respectively Zhang et al. (Ahmadipouya et al., 2021), Feng et al. (Zhang et al., 2019), Ahmad and Ansari (Feng et al., 2021):

$$\frac{C_e}{q_e} = \frac{1}{K_L q_{max}} + \frac{C_e}{q_{max}} \quad (13)$$

$$\ln q_e = \ln K_F + \frac{1}{n_F} \ln C_e \quad (14)$$

$$q_e = \beta_1 \ln K_T + \beta_1 \ln C_e \quad (15)$$

$$\ln q_e = \ln q_s - K \left(RT \ln \left(1 + \frac{1}{C_e} \right) \right)^2 \quad (16)$$

In which q_{max} is the maximum adsorption capacity of theoretical (mg/ g). K_L (L/ mg) is the Langmuir coefficient and is related to the affinity of the binding site. K_F and n_F are Freundlich constants and are related to the capacity and strength of adsorption, respectively (Ahmad and Ansari, 2021; Ahmad and Ejaz, 2022). $1/n_F$ is related to the extent of adsorbent surface heterogeneity. The Temkin isotherm assumes that the absorbed heat decreases linearly with the surface coating, which is the reason for the adsorbent-adsorbate interaction. In Eq. (14), β_1 is the Temkin constant, which represents the absorption of heat, and K_T is the maximum energy band (L/ mg). Also, in the Dubinin-Radushkevich model (Eq. (15)), K , q_s , and ε are adsorption energy, and the theoretical capacity at saturation state and ε is the Polanyi potential, respectively. T is the absolute temperature (K), and R is the universal gas constant ($8.314 \text{ J mol}^{-1} \text{ K}^{-1}$).

In continuation, the effect of the initial concentration of MB and contact time on the removal efficiency of the dye by the adsorbent was investigated, as shown in Fig. 7. As seen from this figure, for different concentrations in the early times, the adsorption intensity is very high, but over time the changes slow down until it finally reaches a constant value, which is called the equilibrium time. Equilibrium times obtained 17, 30, 45, 60, 90, 20 and 15 min for concentrations of 1, 2, 5, 10, 25, 50 and 80 mg/L, respectively.

The Kinetic parameters of the studied models for the adsorption of MB by CMO/C NC are shown in Table 4. The pseudo-first-order model fitted the experimental data better with correlation coefficient (R^2) values of 0.997 and the $q_{e, \text{cal}}$ that was close to the $q_{e, \text{exp}}$.

The isotherm parameters of MB by CMO/C NC have listed in Table 5. By comparing the value of R^2 for different models in Table 5, it is clear that the Langmuir model (0.995) is more consistent with experimental data than other models. In the Langmuir model, it is assumed that the adsorption on the adsorbent surface is monolayer and that the tensile strength of all adsorption centers and sites is the same for MB. Also, the optimal K_L value for the adsorption process based on the Langmuir model is in the range of 0–1, which was obtained at 0.06 in this investigation.

The q_{max} of CuMn₂O₄/chitosan composite for MB was compared to the other adsorbents reported in the literature (Table 6). For instance, the (Algerian) Kaolin applied by Mouni et al. had a significant capacity comparable to that

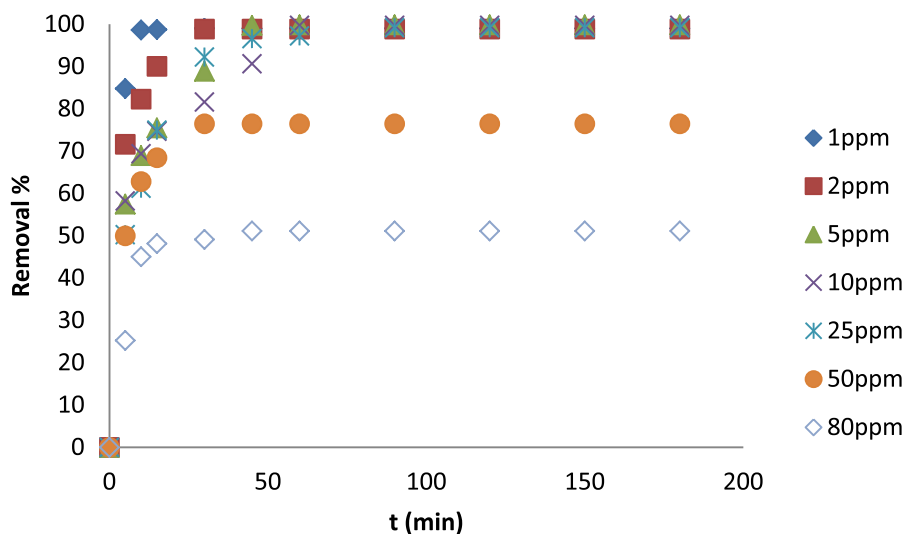


Fig. 7 Effect of contact time and initial concentration on the removal efficiency of MB by CMO/C NC at pH = 6.5 and the ambient temperature.

Table 4 Kinetic parameters for MB removal on CMO/C NCs (experimental conditions: adsorbent dosage = 0.05 g/L; pH = 6.5; concentration = 1 mg/L and agitation speed = 500 rpm).

Pseudo-first order			
$q_{e\text{exp}}(\text{mg/g})$	$q_{e\text{cal}}(\text{mg/g})$	$K_1(1/\text{min})$	R^2
0.792	0.723	0.335	0.997
Pseudo-second order			
$q_{e\text{exp}}(\text{mg/g})$	$q_{e\text{cal}}(\text{mg/g})$	$K_2(\text{g}/\text{mg}\cdot\text{min})$	R^2
0.792	0.634	1.835	0.8981
Intra-particle diffusion			
C	$K_{id}(\text{mg}/\text{g}\cdot\text{min}^{1/2})$		R^2
0.515	0.075		0.819
Elovich			
A (mg/g min)	B (g/mg)		R^2
0.514	0.108		0.578

Table 5 Adsorption isotherm parameters for MB removal on CMO/C NCs (experimental conditions: pH = 6.5; concentration = 1 mg/L; contact time = 5 min and agitation speed = 500 rpm).

Model	Parameter		
Langmuir	$q_{\text{max}}(\text{mg/g})$	$K_L(\text{L}/\text{mg})$	R^2
	54.05	0.06	0.995
Freundlich	$K_F(\text{mg}/\text{g})$	n	R^2
	29.87	0.718	0.8317
Temkin	$K_T(\text{L}/\text{mg})$	β_1	R^2
	49.86	0.8523	0.8033
Dubinin-Radushkevich	$q_{\text{max}}(\text{mg}/\text{g})$	β	R^2
	1.51	0.024	0.5742

obtained in this study (Mouni et al., 2018). Didodecyldimethylammonium bromide-modified brown clay (DDAB-BC) prepared by Munir et al. (Munir et al., 2020) and the activated carbon/cellulose composite (ACC3) used by Somsesta et al.

(Somsesta et al., 2020) showed a strong adsorbent affinity toward MB at higher than ambient temperature with the q_{max} values of 164 (at 55 °C) and 110.35 (at 60 °C) mg/g, respectively. But the chitosan/zeolite composite (Dehghani et al., 2017) and

Table 6 Comparison of the adsorption performances of CMO/C NCs for MB with other adsorbents.

Adsorbent	pH	T (K)	q _{max} (mg/g)	Kinetic model & k; R ²	Isotherm model & K _L or K _F ; R ²	Ref
(Algerian) Kaolin (C ₀ = 80 mg/L)	6	298	52.76	Pseudo-second order 0.037 (g /mg.min) ; 0.997	Langmuir 1.04 (L/mg) ; 0.975	43
Didodecyltrimethylammonium Bromide-Modified Brown Clay (DDAB-BC)	7	328	~ 164	Pseudo-second order 1.128 × 10 ⁻³ (g /mg. min); 0.999	Langmuir 0.899 (L/mg) ; 0.997	44
Activated carbon/cellulose composite (ACC3)	6.9	333	110.35	Pseudo-second order 8.819 × 10 ⁻⁵ (g /mg. min); 0.998	Langmuir 0.239 (L/mg) ; 0.992	45
Chitosan/zeolite composite	9	298	24.5	Pseudo-second order 0.021 (g /mg. min) ; 0.997 (100 mg/L of MB)	Freundlich 8.22 (mg ^{1-1/n} L ^{1/n} /g); 0.999	46
H ₂ SO ₄ crosslinked magnetic chitosan nanocomposite beads (Chit/AILP-Kao) nanocomposite	6	298	20.408	ND	Langmuir 0.018 (L/mg) ; 0.998	47
(Bent/AgNPs-Alg) bio-Nanocomposite	7	303	99.01	pseudo -second order (g /mg. min) ; 0.99	Langmuir 0.04 (L/mg) ; 0.998	48
(Bent/AgNPs-Alg) bio-Nanocomposite	8	303	242.56	pseudo-second-order 0.961	Langmuir 0.986	49
CuMn ₂ O ₄ /chitosan nanocomposite (CMO/C NCs)	6.5	298	54.04	Frist-second order 0.335(1/ min) ; 0.997	Langmuir 0.06 (L/mg) ; 0.995	This work

H₂SO₄ crosslinked magnetic chitosan (Rahmi and Irfan, 2019) showed the q_{max} lower than CuMn₂O₄/chitosan composite that used in this work.

To investigation of desorption and regeneration for the studied adsorbent, the solvents including hydrochloric acid

(HCl), nitric acid (HNO₃), ethanol (C₂H₅OH), acetone ((CH₃)₂CO), sodium hydroxide (NaOH) and distilled water (H₂O)) were used. HCl solution (0.1 M) was selected as a suitable desorbing agents and the highest dye desorption efficiency (72%) was achieved by HCl solution. The results showed that after 5 cycles, the absorption of MB reached 42%, therefore the adsorbent can be effectively used up to five adsorption/desorption cycles (Fig. 8).

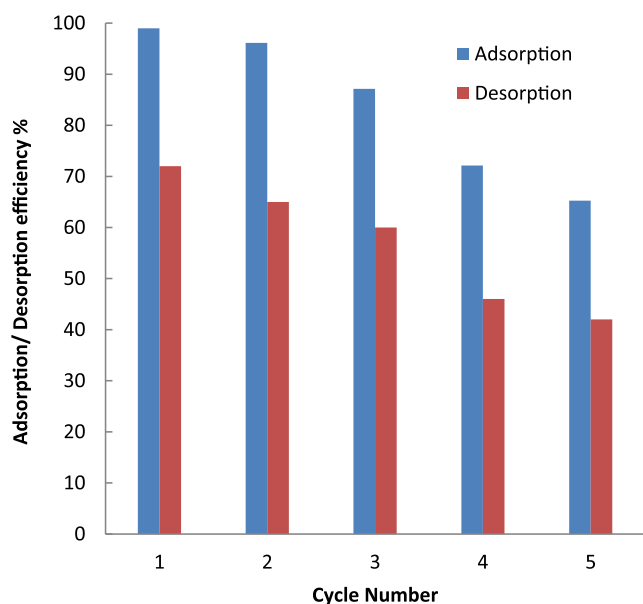


Fig. 8 Plot adsorption/desorption of MB versus cycle number (contact time = 5 min, initial dye concentration = 1 mg/L, solvent = HCl, and dosage of adsorbent = 1.25 g/L).

4. Conclusions

The CuMn₂O₄ nanostructures and micro/nanocomposites were synthesized in the presence of onion as a capping agent, for the first time to our knowledge. The VSM, UV-Vis, and FT-IR results have enabled us to determine the magnetic and optical behaviors of the NCs. The as-prepared CMO/C NCs were efficient adsorbents for the MB removal from an aqueous solution. Before and after the adsorption of MB on the surface of the composite, FT-IR spectra of the composite were similar, and only peaks were blue-shifted in the spectrum of the composite after MB absorption. In both UV-Vis and FT-IR spectra, the peaks of MB disappeared after its adsorption on the surface of the CMO/C NCs. The MB removal efficiency increased by decreasing the MB concentration from 80 mg/L to 1 mg/L. The maximum removal efficiency was 99% and obtained at 1 mg/L concentration. The equilibrium time of the adsorption process decreased by increasing the concentration of MB solution. It can be due to the high accumulation of MB around the adsorbent and increase the chance of it colliding with the adsorbent. Therefore, in this case, the determining factor of equilibrium time is the adsorbent capacity. However, at low concentrations, the determining factor of equilibrium time was the MB concentration in the solution. This work is the first report of MB removal by absorption on the surface of CMO/C NCs.

Declaration of Competing Interest

The authors declare that they have no known competing financial interests or personal relationships that could have appeared to influence the work reported in this paper.

Acknowledgment

Authors are grateful to the Kosar University of Bojnord for supporting this work.

References

- Abel, M.J., Pramothkumar, A., Senthilkumar, N., Jothivenkatachalam, K., Inbaraj, P.F.H., Prince, J.J., 2019. Flake-like CuMn_2O_4 nanoparticles synthesized via co-precipitation method for photocatalytic activity. *Phys B (Amsterdam, Neth.)* 572, 117–124.
- Ahmad, R., Ansari, K.h., 2021. Comparative study for adsorption of congo red and methylene blue dye on chitosan modified hybrid nanocomposite. *Process Biochem.* 108, 90–102.
- Ahmad, R., Ejaz, M.O., 2022. Adsorption of methylene blue dye from aqueous solution onto synthesized bentonite/silvernanoparticles-alginate (Bent/AgNPs-Alg) bio-nanocomposite. *Biomass Conv. Bioref.*
- Ahmad, R., Kumar, R., 2010. Adsorption studies of hazardous malachite green onto treated ginger waste. *J. Env. Manage.* 01, 1032–1038.
- Ahmadi, A., Foroutan, R., Esmaeili, H., Peighambar-doust, S.J., Hemmati, S., Ramavandi, B., 2022. Montmorillonite clay/starch/ CoFe_2O_4 nanocomposite as a superior functional material for uptake of cationic dye molecules from water and wastewater. *Mater. Chem. Phys.* 284, 126088.
- Ahmadijokani, F., Mohammadkhani, R., Ahmadipouya, S., Shokrgozar, A., Rezakazemi, M., Molavi, H., Aminabhavi, T.M., Arjmand, M., 2020. Superior chemical stability of UiO-66 metal-organic frameworks (MOFs) for selective dye adsorption. *Chem. Eng. J.* 399, 125346.
- Ahmadipouya, S., Heidarian Haris, M., Ahmadijokani, F., Jarahiyan, A., Molavi, H., Matloubi Moghaddam, F., Rezakazemi, M., Arjmand, M., 2021. Magnetic $\text{Fe}_3\text{O}_4@ \text{UiO}-66$ nanocomposite for rapid adsorption of organic dyes from aqueous solution. *J. Mol. Liq.* 322, 114910.
- Alizadeh, M., Peighambar-doust, S.J., Foroutan, R., Azimi, H., Ramavandi, B., 2022. Surface magnetization of hydrolyzed Luffa Cylindrica biowaste with cobalt ferrite nanoparticles for facile Ni^{2+} removal from wastewater. *Environ. Res.* 212, 113242.
- Allègre, C., Moulin, P., Maisseu, M., Charbit, F., 2006. Treatment and reuse of reactive dyeing effluents. *J. Membr. Sci.* 269, 15–34.
- Bhatnagar, A., Sillanpää, M., 2009. Applications of chitin- and chitosan-derivatives for the detoxification of water and wastewater—A short review. *Adv. Colloid. Interface.* 152, 26–38.
- Buhl, R., 1969. Manganites spinelles purs d'elements de transition preparations et structures cristallographiques. *J. Phys. Chem. Solids* 30, 805–812.
- Chani, M.T.S., Karimov, K.S., BahadarKhan, S., Fatima, N., Asiri, A.M., 2019. Impedimetric humidity and temperature sensing properties of chitosan- CuMn_2O_4 spinel nanocomposite. *Ceram. Int.* 45, 10565–10571.
- Dehghani, M.H., Dehghan, A., Alidadi, H., Dolatabadi, M., Mehrabpour, M., Converti, A., 2017. Removal of methylene blue dye from aqueous solutions by a new chitosan/zeolite composite from shrimp waste: Kinetic and equilibrium study. *Korean J. Chem. Eng.* 34, 1699–1707. IITED.
- Emadi, H., Salavati-Niasari, M., Sobhani, A., 2017. Synthesis of some transition metal (M: 25Mn, 27Co, 28Ni, 29Cu, 30Zn, 47Ag, 48Cd) sulfide nanostructures by hydrothermal method. *Adv. Colloid Interface Sci.* 246, 52–74.
- Enhessari, M., Salehabadi, A., Maarofian, K., Khanahmadzadeh, S., 2016. Synthesis and physicochemical properties of CuMn_2O_4 nanoparticles; a potential semiconductor for photoelectric devices. *Int. J. Bio-Inorg. Hybr. Nanomater.* 5, 115–120.
- Far, H.S., Hasanzadeh, M., Nashtaei, M.S., Rabbani, M., Haji, A., Hadavi Moghadam, B., 2020. PPI-Dendrimer-Functionalized magnetic metal-organic framework $\text{Fe}_3\text{O}_4@ \text{MOF} @ \text{PPI}$ with high adsorption capacity for sustainable wastewater treatment. *ACS Appl. Mater. Interfaces* 12, 25294–25303.
- Feng, M., Yu, S., Wu, P., Wang, Z., Liu, S., Fu, J., 2021. Rapid, high-efficient and selective removal of cationic dyes from wastewater using hollow polydopamine microcapsules: isotherm, kinetics, thermodynamics and mechanism. *Appl. Surf. Sci.* 542, 148633.
- Fereidonian Dashti, A., Adlan, M.N., Abdul Aziz, H., Ibrahim, A.H., 2018. Application of response surface methodology (RSM) for optimization of ammoniacal nitrogen removal from palm oil mill wastewater using limestone roughing filter. *J. Appl. Res. Water Wastewater* 5, 411–416.
- Foroutan, R., Peighambar-doust, S.J., Esvandi, Z., Khatooni, H., Ramavandi, B., 2021. Evaluation of two cationic dyes removal from aqueous environments using CNT/MgO/CuFe₂O₄ magnetic composite powder: A comparative study. *J. Env. Chem. Eng.* 9, 104752.
- Foroutan, R., Peighambar-doust, S.J., Mohammadi, R., Peighambar-doust, S.H., Ramavandi, B., 2022. Cadmium ion removal from aqueous media using banana peel biochar/ $\text{Fe}_3\text{O}_4@ \text{ZIF}-67$. *Environ. Res.* 211, 113020.
- Foroutan, R., Peighambar-doust, S.J., Mohammadi, R., Peighambar-doust, S.H., Ramavandi, B., 2022. Development of new magnetic adsorbent of walnut shell ash/starch/ Fe_3O_4 for effective copper ions removal: Treatment of groundwater samples. *Chemosphere* 296, 133978.
- Gollakota, A.R.K., Munagapati, V.S., Volli, V., Gautam, S., Wen, J. C., Shu, C.M., 2021. Coal bottom ash derived zeolite (SSZ-13) for the sorption of synthetic anion Alizarin Red S (ARS) dye. *J. Hazard Mater.* 416, 125925.
- Guimaraes, T., Paquini, L.D., Lyrio Ferraz, B.R., Roberto Profeti, L. P., Profeti, D., 2020. Efficient removal of Cu(II) and Cr(III) contaminants from aqueous solutions using marble waste powder. *J. Environ Chem. Eng.* 8, 103972.
- Holkar, C.R., Jadhav, A.J., Pinjari, D.V., Mahamuni, N.M., Pandit, A.B., 2016. A critical review on textile wastewater treatments: possible approaches. *J. Environ. Manag.* 182, 351–366.
- Hutchings, G.J., Mirzaei, A.A., Joyner, R.W., Siddiqui, M.R.H., Taylor, S.H., 1996. Ambient temperature CO oxidation using copper manganese oxide catalysts prepared by co-precipitation: effect of ageing on catalyst performance. *Catal. Lett.* 42, 21–24.
- Julinová, M., Slavík, R., 2012. Removal of phthalates from aqueous solution by different adsorbents: A short review. *J. Environ. Manage.* 94, 13–24.
- Khan, A.A., Molla, A., Chowdhury, A., Kumari, S., Hussain, S., 2021. Surface-charge-controlled synthesis of ZnIn_2S_4 nanosheet-based materials for selective adsorption of organic dyes. *ACS Appl. Nano Mater.* 4, 4114–4128.
- Khatooni, H., Peighambar-doust, S.J., Foroutan, R., Mohammadi, R., Ramavandi, B., 2023. Adsorption of methylene blue using sodium carboxymethyl cellulose-g-poly (acrylamide-co-methacrylic acid)/Cloisite 30B nanocomposite hydrogel. *J. Polym. Environ.* 31, 297–311.
- Kumar, M.N.V.R., 2000. A review of chitin and chitosan applications. *React. Funct. Polym.* 46, 1–27.
- Ma, P., Geng, Q., Gao, X., Yang, S., Liu, G., 2016. Solution combustion of spinel CuMn_2O_4 ceramic pigments for thickness sensitive spectrally selective (TSSS) paint coatings. *Ceram. Int.* 42, 11966–11973.

- Marrot, B., Roche, N., 2002. Wastewater treatment and reuse in textile industries, A review. *Res. Adv. Water Res.* 3, 41–53.
- Mouni, L., Belkhir, L., Bollinger, J.C., Bouzaza, A., Assadi, A., Tirri, A., Dahmoune, F., Madani, K., Remini, H., 2018. Removal of Methylene Blue from aqueous solutions by adsorption on Kaolin: Kinetic and equilibrium studies. *Appl. Clay Sci.* 153, 38–45.
- Munir, M., Nazar, M.F., Zafar, M., Zubair, M., Ashfaq, A., Hosseini-Bandegharai, S., Khan, A.A., 2020. Effective Adsorptive Removal of Methylene Blue from Water by Didodecyltrimethylammonium Bromide-Modified Brown Clay. *ACS Omega* 5, 16711–16721.
- Pamukoglu, M.Y., Kargi, F., 2006. Batch kinetics and isotherms for biosorption of copper(II) ions onto pre-treated powdered waste sludge (PWS). *J. Hazard. Mater.* 138, 479–484.
- Pamukoglu, M.Y., Kargi, F., 2007. Effects of operating parameters on kinetics of copper(II) ion biosorption onto pre-treated powdered waste sludge (PWS). *Enzyme Microb. Technol.* 42, 76–82.
- Popescu, I., Boudjema, A., Helaili, N., Bessekhoud, Y., Tudorache, M., Bachari, K., Marcu, I.C., 2015. Study of the electrical and catalytic properties of spinels with CuFe_{2-x}Mn_xO₄ composition (x = 0, 0.4, 0.8, 1.6 and 2). *Appl. Catal. A: Gen.* 504, 29–36.
- Radhakrishnan, N.K., Biswas, A.B.A., 1974. Neutron diffraction study of cation distributions in some manganites. *J. Indian Chem. Soc.* 51, 274–280.
- Rahmi, I., Irfan, M., 2019. Methylene blue removal from water using H₂SO₄ crosslinked magnetic chitosan nanocomposite beads. *Microchem. J.* 144, 397–402.
- Reddy, D.H.K., Lee, S.-M., 2013. Synthesis and characterization of a chitosan ligand for the removal of copper from aqueous media. *J. Appl. Polym. Sci.* 130, 4542–4550.
- Rowshanzamir, S., Peighambari, S.J., Parnian, M.J., Amirkhani, G.R., Rahnavard, A., 2015. Effect of Pt-Cs₂.5H₀.5PW12O₄₀ catalyst addition on durability of self-humidifying nanocomposite membranes based on sulfonated poly (ether ether ketone) for proton exchange membrane fuel cell applications. *Int. J. Hydrogen Energy* 40, 549–560.
- Safarzadeh, H., Peighambari, S.J., Mousavi, S.H., Foroutan, R., Mohammadi, R., Peighambari, S.H., 2022. Adsorption ability evaluation of the poly(methacrylic acid-co-acrylamide)/cloisite 30B nanocomposite hydrogel as a new adsorbent for cationic dye removal. *Environ. Res.* 212, 113349.
- Salavati-Niasari, M., Sobhani, A., 2013. Effect of nickel salt precursors on morphology, size, optical property and type of products (NiSe or Se) in hydrothermal method. *Opt. Mat.* 35, 904–909.
- Sheikhzadeh, M., Sanjabi, S., 2021. Coelectrodeposition of crystalline copper-manganese oxide containing CuMn₂O₄ spinel for high energy supercapacitor application. *Synth. Met.* 278, 116802–116804.
- Shoemaker, D.P., Li, J., Seshadri, R., 2009. Unraveling atomic positions in an oxide spinel with two Jahn–Teller Ions: local structure investigation of CuMn₂O₄. *J. Am. Chem. Soc.* 131, 11450–11457.
- Sinha, A.P.B., Sanjana, N.R., Biswas, A.B., 1958. The crystal structure of copper manganite. *J. Phys. Chem. B.* 62, 191–194.
- Sobhani, A., 2022. Hydrothermal synthesis of CuMn₂O₄/CuO nanocomposite without capping agent and study its photocatalytic activity for elimination of dye pollution. *Int. J. Hydrogen Energy* 47, 20138–20152.
- Sobhani, A., Salavati-Niasari, M., 2014. Synthesis and characterization of a nickel selenide series via a hydrothermal process. *Superlattices Microstruct.* 65, 79–90.
- Sobhani, A., Salavati-Niasari, M., 2015. Synthesis and characterization of FeSe₂ nanoparticles and FeSe₂/FeO (OH) nanocomposites by hydrothermal method. *J. Alloys Compd.* 625, 26–33.
- Sobhani, A., Salavati-Niasari, M., Davar, F., 2012. Shape control of nickel selenides synthesized by a simple hydrothermal reduction process. *Polyhedron* 31, 210–216.
- Sobhani, A., Salavati-Niasari, M., 2021. Transition metal selenides and diselenides: Hydrothermal fabrication, investigation of morphology, particle size and their applications in photocatalyst. *Adv. Colloid Interface Sci.* 287, 102321–102343.
- Somsesta, N., Sricharoenchaikul, V., Aht-Ong, D., 2020. Adsorption removal of methylene blue onto activated carbon/cellulose biocomposite films: Equilibrium and kinetic studies. *Mater. Chem. Phys.* 240, 122221.
- Tehrani-Bagha, A.R., Nikkar, H., Mahmoodi, N.M., Markazi, M., Menger, F.M., 2011. The sorption of cationic dyes onto kaolin: kinetic, isotherm and thermodynamic studies. *Desalination* 266, 274–280.
- Travlou, N.A., Kyzas, G.Z., Lazaridis, N.K., Deliyanni, E.A., 2013. Functionalization of graphite oxide with magnetic chitosan for the preparation of a nanocomposite dye adsorbent. *Langmuir* 29, 1657–1668.
- Vandenbergh, R.E., Robbrect, G.G., Brabers, V.A.M., 1976. Structure and ionic configuration of oxidic copper-manganese spinels (Cu_xMn_{3-x}O₄). *Phys. Status Solidi A* 34, 583–592.
- Verwey, E.J.W., Heilmann, E.L., 1947. Physical properties and cation arrangement of oxides with spinel structures I. Cation arrangement in spinels. *J. Chem. Phys.* 15, 174–180.
- Verwey, E.J.W. 1951. Oxidic semiconductors in semi-conducting materials. In: Henisch, H.K., (Ed.), Butterworths Sc, Pub Ltd.: London, UK, p. 151.
- Wang, Y., He, L., Li, Y., Jing, L., Wang, J., Li, X., 2020. Ag NPs supported on the magnetic Al-MOF/PDA as nanocatalyst for the removal of organic pollutants in water. *J. Alloys Compd.* 828, 154340.
- Wang, L.J., Zhou, Q., Liang, Y., Shi, H., Zhang, G., Wang, B., Zhang, W., Lei, B., Wang, W.Z., 2013. Size effect and enhanced photocatalytic activity of CuO sheet-like nanostructures prepared by a room temperature solution phase chemical method. *Appl. Surf. Sci.* 271, 136–140.
- Waskowska, A., Gerward, L., Olsen, J.S., Steenstrup, S., Talik, E., 2001. CuMn₂O₄: properties and the high-pressure induced Jahn–Teller phase transition. *J. Phys.: Condens. Matter.* 13, 2549–2562.
- Wollner, A., Lange, F., Schemelz, H., Knozinger, H., 1993. Characterization of mixed copper-manganese oxides supported on titania catalysts for selective oxidation of ammonia. *Appl. Catal. A: Gen.* 94, 181–203.
- Yao, B., Ni, C., Xiong, C., Zhu, C., Huang, B., 2010. Hydrophobic modification of sodium alginate and its application in drug controlled release. *Bioprocess Biosyst. Eng.* 33, 457–463.
- Yin, G., Song, X., Tao, L., Sarkar, B., Sarmah, A.K., Zhang, W., Lin, Q., Xiao, R., Liu, Q., Wang, H., 2020. Novel Fe-Mn binary oxide-biochar as an adsorbent for removing Cd (II) from aqueous solutions. *Chem. Eng. J.* 389, 124465.
- Zhang, Z., Chen, H., Wu, W., Pang, W., Yan, G., 2019. Efficient removal of Alizarin Red S from aqueous solution by polyethyleneimine functionalized magnetic carbon nanotubes. *Bioresour. Technol.* 93, 122100.
- Zhang, C., Xie, A., Zhang, W., Chang, J., Liu, C., Gu, L., Duo, X., Pan, F., Luo, S., 2021. CuMn₂O₄ spinel anchored on graphene nanosheets as a novel electrode material for supercapacitor. *J. Energy Storage* 34, 102181–102183.
- Zhu, H.Y., Jiang, R., Xiao, L., Zeng, G.M., 2010. Preparation, characterization, adsorption kinetics and thermodynamics of novel magnetic chitosan wrapping nanosized γ-Fe₂O₃ and multi-walled carbon nanotubes with enhanced adsorption properties for methyl orange. *Bioresour. Technol.* 101, 5063–5069.